Absolute cross sections and kinetic energy release for doubly and triply charged fragments produced by electron impact on CO^+

2007 J. Phys. B: At. Mol. Opt. Phys. 40 85

(http://iopscience.iop.org/0953-4075/40/1/008)

INSTITUTE OF PHYSICS PUBLISHING JOURNAL OF PHYSICS B: ATOMIC, MOLECULAR AND OPTICAL PHYSICS

J. Phys. B: At. Mol. Opt. Phys. **40** (2007) 85–100 doi:10.1088/0953-4075/40/1/008

Absolute cross sections and kinetic energy release for doubly and triply charged fragments produced by electron impact on CO^+

J Lecointre[1], D S Belic[2], J J Jureta[1,3], K Becker[4], H Deutsch[5], J Limtrakul[6], T D Märk[7,8], M Probst[7] and P Defrance[1]

[1] Département de Physique, Université Catholique de Louvain, unité PAMO, Chemin du Cyclotron 2, B-1348 Louvain-la-Neuve, Belgium
[2] Faculty of Physics, PO Box 386, 11000 Belgrade, Serbia
[3] Institute of Physics, PO Box 68, 11081, Belgrade, Serbia
[4] Department of Physics and Center for Environmental Systems, Stevens Institute of Technology, Hoboken, NJ 07030, USA
[5] Institut für Physik, Ernst Moritz Arndt Universität Greifswald, Domstr. 10a, D-17487 Greifswald, Germany
[6] Department of Chemistry, Kasetsart University, Bangkok 10900, Thailand
[7] Institut für Ionenphysik, Leopold Franzens Universität Innsbruck, Technikerstr. 25, A-6020 Innsbruck, Austria
[8] Department of Plasmaphysics, Univerzita Komenskeho, Mlynska dolina, 842 48 Bratislava 4, Slovak Republic

Received 18 September 2006, in final form 26 October 2006
Published 19 December 2006
Online at stacks.iop.org/JPhysB/40/85

Abstract

Absolute cross sections for electron impact ionization of CO^+ leading to the formation of doubly and triply charged products (CO^{2+}, C^{2+} and O^{2+}, C^{3+} and O^{3+}) are reported in the energy range from their respective thresholds to 2500 eV. Around the maximum, cross section values are found to be $(13.36 \pm 0.56) \times 10^{-18}$ cm^2, $(5.58 \pm 0.55) \times 10^{-18}$ cm^2 and $(1.37 \pm 0.14) \times 10^{-18}$ cm^2 for CO^{2+}, C^{2+} and O^{2+}, respectively, and $(28.3 \pm 7.0) \times 10^{-21}$ cm^2 and $(2.4 \pm 0.7) \times 10^{-21}$ cm^2 for C^{3+} and O^{3+}, respectively. The analysis of ionic product velocity distributions, obtained by means of a crossed electron–ion beam set-up, allows the determination of the kinetic energy release distributions. They are seen to extend from 0 to 50 eV both for C^{2+} and O^{2+}. The mean kinetic energy releases for C^{3+} and O^{3+} are found to be 33 ± 5 eV and 39 ± 9 eV, respectively. The cross sections are seen to depend exponentially on the potential energy of each dissociated ion pair. The total single CO^+ ionization cross section calculated by application of the Deutsch–Märk (DM) formalism is found to be in good agreement with the experimental results.

1. Introduction

Ionization of molecules by electron impact is of great importance in atmospheric science, plasma processing and mass spectroscopy. Important energy loss processes for energetic electrons occur by collisions of electrons with carbon monoxide gas in many astrophysical environments and in planetary atmospheres, for example the Halley comet or the planet Mars (Liu and Victor 1994). Despite the fact that doubly charged ions of diatomic molecules have been known to exist for several decades (Dorman and Morrison 1961), the high density of electronic states involved implies that accurate electronic structure calculations are difficult, and consequently, the knowledge of the properties of these systems is still ambiguous.

The carbon monoxide dication has been investigated by a number of experimental methods: Auger spectroscopy (e.g. Curtis and Boyd (1984), Moddeman *et al* (1971)), electron impact (Hille and Märk 1978), double charge transfer (Mazumdar *et al* 1988), photoion–fluorescence photon coincidence (PIFCO; Dujardin *et al* 1990), threshold photoelectron coincidence spectroscopy (TEPsCO; Hall *et al* 1992) and ion storage ring (Andersen *et al* 1993).

Experiments of electron interaction with CO^+ have been carried out previously in our laboratory (Belic *et al* 1997): single ionization (SI, CO^{2+} formation) and asymmetric dissociative ionization (doubly-charged products, C^{2+} and O^{2+}, formation). A reanalysis of the former results indicated that the angular divergence of dissociation products was not properly controlled in that experiment, inducing an important underestimation of the corresponding cross sections. Very recently (Lecointre *et al* 2006), cross sections were reported for singly-charged ions produced via dissociative excitation (DE, $C^+ + O$ and $C + O^+$) and dissociative ionization (DI, $C^+ + O^+$). These results were obtained by means of a renewed experimental set-up, which was built to avoid the above-mentioned problems associated with the angular divergence. The experimental method was extended in order to also determine kinetic energy release distributions (KERDs) at selected electron energies.

As a consequence, the study of the doubly-charged products (CO^{2+}, C^{2+} and O^{2+}) has been repeated. In addition, for the first time in our laboratory, the formation of the triply-charged products was observed in the energy range from threshold up to 2.5 keV. To summarize, the following reactions are investigated in the present paper:

$$CO^+ + e^- \rightarrow CO^{2+} + 2e^- \quad \sigma_1 \tag{1}$$

$$\rightarrow C^{2+} + \cdots \quad \sigma_2 \tag{2}$$

$$\rightarrow O^{2+} + \cdots \quad \sigma_3 \tag{3}$$

$$CO^+ + e^- \rightarrow C^{3+} + \cdots \quad \sigma_4 \tag{4}$$

$$\rightarrow O^{3+} + \cdots \quad \sigma_5. \tag{5}$$

In the following section, the experimental set-up, the experimental procedure and the data analysis method are briefly described. Section 3 is devoted to the presentation and the discussion of the results (cross sections and KERDs) obtained for reactions (1)–(5).

2. Apparatus and experimental method

In this experiment, the animated crossed electron–ion beam method is applied (Defrance *et al* 1981). Both the present apparatus and the experimental method have recently been described in detail (Lecointre *et al* 2006) and only a brief outline is presented here.

2.1. Experimental set-up

In the apparatus, the fixed energy molecular ion beam interacts at right angles with an electron beam whose energy may be tuned from a few electron-volts up to 2.5 keV. Ions are extracted from an ECR ion source and accelerated to 12 keV. The ion beam is mass-selected by means of a double focusing 90° magnetic analyser, additionally focused and purified by a 45° spherical electrostatic deflector, and directed into the collision region where it crosses the ribbon-shaped electron beam. Product ions are separated from the primary ion beam by means of a double focusing 90° magnetic analyser. Due to the transfer of internal potential energy, dissociation fragments exhibit both a broad velocity and angular distributions in the laboratory frame. At a fixed ion velocity, selected by the variable analyser slit, the angular acceptance of the magnet (0.1 rad) is large enough to convey to the detector all the ions with the maximum expected kinetic energy release (KER) produced by dissociation processes. Product ions are further deflected by a 90° electrostatic spherical deflector and directed onto a channeltron detector.

2.2. Cross section measurements

In the animated beam method (Defrance *et al* 1981), the electron beam is swept across the ion beam in a linear see saw motion at a constant speed u. The total number of events K produced during one complete electron beam movement is related to the cross section (σ) by the following expression:

$$\sigma = \frac{uK}{AI_eI_i\gamma} \tag{6}$$

where γ is the detector efficiency, I_e and I_i are the electron and ion beam current intensities, respectively, and the kinematic factor (A), for beams interacting at right angles, is given by

$$A = \frac{\left(v_e^2 + v_i^2\right)^{1/2}}{v_e v_i q_i e^2}. \tag{7}$$

In this expression, e and q_ie, v_e and v_i are the charges and velocities of electrons and ions, respectively. Assuming $m_i \gg m_e$, the true interaction energy E_e (eV) is given by

$$E_e = V_e + \frac{m_e}{m_i}(q_iV_i - V_e) \tag{8}$$

where V_e and V_i, m_e and m_i are the acceleration voltages and masses of electrons and ions, respectively. The electron energy is corrected for the contact potential.

2.3. Kinetic energy release distributions

The angular acceptance of the magnet analyser allows the total transmission of the angular distribution of product fragments emitted at a given velocity v in the laboratory frame. This velocity depends on B ($v = qRB/m$) and is also related to $\sqrt{v_c^2 + w^2 + 2v_cw\cos\theta_L}$, where v_c, θ_L and w represent the centre-of-mass velocity, the ejection angle in the laboratory and the fragment velocity in the centre of mass frame, respectively. Here, m and q are the fragment ion mass and charge, respectively, and R is the radius of its trajectory in the analyser magnetic field.

The velocity distribution usually exceeds the corresponding acceptance defined by the limited size of the analyser slits. As a consequence, the transmission of dissociation products is only partial and the velocity distribution ($d\sigma(v)/dv$) may be obtained by measuring the apparent cross section $\sigma_m(B)$ as a function of the analyser magnetic field (B) at a given electron energy. The corresponding differential cross section, $f(B) = d\sigma(B)/dB$, is determined via a

specific procedure (Lecointre *et al* 2006) and consequently, the velocity distribution is given by

$$\frac{\mathrm{d}\sigma(v)}{\mathrm{d}v} = \frac{m}{qR}\frac{\mathrm{d}\sigma(B)}{\mathrm{d}B}. \tag{9}$$

Lecointre *et al* (2006) demonstrated that the KERD may be expressed in terms of the velocity distribution by

$$\frac{\mathrm{d}\sigma(E_{\mathrm{KER}})}{\mathrm{d}E_{\mathrm{KER}}} = \frac{-2\mu v_{\mathrm{c}}}{m^2(1-\varepsilon/2)}\frac{\mathrm{d}}{\mathrm{d}v}\left(\frac{1}{v}\frac{\mathrm{d}\sigma(v)}{\mathrm{d}v}\right) \tag{10}$$

where μ is the reduced mass of the fragment. In the present experiment, ε is expressed as

$$\varepsilon = 2\left(1 - \frac{2v_{\mathrm{c}}}{\sigma}\int_{v_{\mathrm{c}}}^{\infty}\frac{1}{v}\frac{\mathrm{d}\sigma(v)}{\mathrm{d}v}\,\mathrm{d}v\right). \tag{11}$$

This quantity is seen to characterize the angular distribution of dissociation products with respect to the velocity of the incident electron, due to the initial orientation of the molecule.

The total kinetic energy released (E_{KER}) to dissociation fragments is given by

$$E_{\mathrm{KER}} = \frac{m^2w^2}{2\mu}. \tag{12}$$

2.4. Experimental procedure

At a fixed v, only a fraction (η) of the fragment velocity distribution is detected at the same time. To overcome this problem, the above-mentioned magnetic field scans are performed and the total cross section is computed by

$$\sigma = \int_{-\infty}^{+\infty} f(B)\,\mathrm{d}B. \tag{13}$$

The repetition of this procedure at each electron energy results in a very long and tedious task. In order to reduce this task with little effect on the accuracy of final results, an alternative procedure (Bahati *et al* 2001) was introduced to cover the whole energy range without measuring all the distributions. In the first step, the apparent cross section $\sigma_{\mathrm{m}}(B_0)$ is measured versus the electron energy at the magnetic field B_0 which corresponds to the centre of the velocity distribution, that is to the detection of fragments with $v = v_{\mathrm{c}}$. Working at this field is necessary in order to include the contributions of all the ejection speeds in the centre-of-mass frame. The apparent cross section is related to σ by

$$\sigma_{\mathrm{m}}(B_0) = \eta\sigma. \tag{14}$$

To put the apparent cross section $\sigma_{\mathrm{m}}(B_0)$ on the absolute scale over the whole electron energy range, the transmission factor η is determined in a second step as follows. On the one hand, it is computed at the selected energies where magnetic field scans are performed. On the other hand, it is estimated over the whole energy range by interpolation and extrapolation of these results. Finally, the apparent cross sections are corrected by means of (14) to obtain the absolute cross sections in the whole energy range.

Typical working conditions are the following: ion current 300 nA, electron current 0.5–2.5 mA, electron beam sweeping speed 3.75 m s^{-1}, number of events per one sweep 0.1. The pressure is kept below 1×10^{-9} mbar in the collision chamber during the measurement, in order to reduce the background. The energy of the ion beam (12 keV) is high enough to ensure 100% detection efficiency of the channeltron detector.

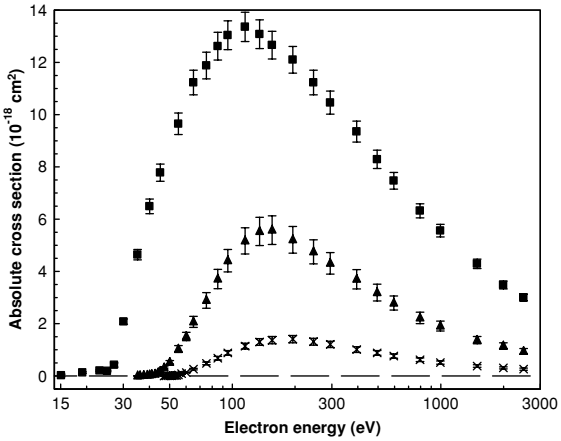

Figure 1. Absolute cross sections for the production of CO^{2+} (σ_1, ■), C^{2+} (σ_2, ▲) and O^{2+} (σ_3, ×) versus electron energy.

The uncertainty associated with the transmission factor is estimated to be 5%. The total uncertainty (90% confidence limit) is obtained as the square root of the quadratic sum of the statistical and systematic uncertainties at the cross section maximum (Lecointre *et al* 2006). Consequently, the total uncertainty is found to be 4.2% for single ionization σ_1, 9.4% for doubly charged fragments (i.e. σ_2 and σ_3) and 18.8% for triply charged fragments (i.e. σ_4 and σ_5).

3. Results and discussion

Absolute cross sections (σ_1–σ_5, reactions (1)–(5)) have been obtained for the formation of CO^{2+}, C^{2+}, O^{2+}, C^{3+} and O^{3+}. They are listed in tables 1 and 2 together with the corresponding electron energies and the total associated uncertainties (90% confidence limit). KERDs are obtained for dissociation products at selected electron energies only.

3.1. Doubly charged products

3.1.1. Single ionization: CO^{2+} production. In the ionization process, the CO^{2+} ions are formed in states which are unstable towards dissociation. The lifetimes of the lowest states were measured by several groups: CO^{2+} lifetimes were estimated to the range between 9 and 30 μs (Newton and Sciamanna 1970, Hirsch *et al* 1975, Curtis and Boyd 1984). Wetmore *et al* (1984) calculated values ranging from approximately 10^{-8} to 10^{-4} s. A storage ring experiment (Andersen *et al* 1993) demonstrated that these lifetimes may extend up to 3.8 s for the lowest $^3\Pi_I$ ($v = 0$) state. In the present experiment, CO^{2+} fragments spend a few microseconds flying from the collision region to the detector, so that only ions with the lifetime longer than this time-of-flight are detected.

The maximum of σ_1 is found to be $(13.36 \pm 0.56) \times 10^{-18}$ cm^2 at 115.1 eV electron energy (figure 1). The present threshold energy for this process is estimated to be (26.7 ± 0.5) eV relative to the ground state of CO^+ (table 3). These results are similar to those obtained by Belic *et al* (1997), who found the threshold to be (27.0 ± 0.5) eV and the maximum cross section was $(14.50 \pm 0.62) \times 10^{-18}$ cm^2 around 134 eV. This indicates that both sets of SI data are in very good agreement with each other, keeping in mind that the uncertainty on previous results (0.62) was also estimated at the 90% confidence limit.

Table 1. Absolute cross sections for CO^{2+}, C^{2+} and O^{2+} formation (10^{-18} cm^2) (90% confidence limit).

	CO^{2+}		C^{2+}		O^{2+}	
E_e (eV)	σ_1	$\Delta\sigma_1$	σ_2	$\Delta\sigma_2$	σ_3	$\Delta\sigma_3$
15.1	0.02	0.05				
19.1	0.13	0.03				
23.1	0.20	0.03				
25.1	0.19	0.03				
27.1	0.42	0.08				
30.1	2.08	0.10				
35.1	4.64	0.20	0.000	0.005		
36.1			0.007	0.005		
37.6			0.02	0.02		
39.1			0.03	0.02		
40.1	6.49	0.28	0.04	0.02		
41.1			0.05	0.02		
42.6			0.07	0.02		
44.1			0.12	0.03		
45.1	7.78	0.33	0.18	0.04		
47.1			0.31	0.04	0.000	0.005
48.1					0.003	0.005
49.1					0.007	0.005
50.1			0.52	0.07	0.005	0.008
51.1					0.006	0.008
52.1					0.011	0.008
53.1					0.015	0.008
54.1					0.02	0.02
55.1	9.65	0.41	1.03	0.13	0.04	0.02
57.1					0.09	0.02
60.1			1.51	0.16	0.13	0.02
65.1	11.23	0.47	2.07	0.21	0.26	0.03
75.1	11.88	0.51	2.89	0.30	0.48	0.05
85.1	12.62	0.53	3.71	0.37	0.68	0.07
95.1	13.04	0.55	4.41	0.43	0.88	0.09
115.1	13.36	0.56	5.17	0.50	1.14	0.11
135.1	13.08	0.55	5.53	0.54	1.30	0.13
155.1	12.66	0.53	5.58	0.55	1.37	0.14
195.1	12.10	0.51	5.21	0.51	1.41	0.14
245.1	11.23	0.47	4.75	0.46	1.31	0.13
295.1	10.46	0.44	4.31	0.41	1.21	0.12
395.1	9.35	0.40	3.70	0.37	1.01	0.11
495.1	8.29	0.35	3.19	0.32	0.88	0.09
595.1	7.47	0.32	2.79	0.27	0.76	0.08
795.1	6.32	0.27	2.22	0.22	0.62	0.07
995.1	5.56	0.24	1.91	0.19	0.51	0.06
1495.1	4.29	0.18	1.37	0.14	0.38	0.05
1995.1	3.48	0.15	1.15	0.12	0.31	0.04
2495.1	3.00	0.13	0.94	0.11	0.26	0.04

Various studies of the neutral molecule have been carried out giving access to the CO^{2+} appearance potential value ($^3\Pi_I$, $v = 0$ state) relative to the ground state ($X^1\Sigma$ $v = 0$). The CO^+ single ionization threshold is obtained by subtracting the single ionization threshold

Table 2. Absolute cross sections for C^{3+} and O^{3+} formation (10^{-21} cm^2) (90% confidence limit).

	C^{3+}		O^{3+}	
E_e (eV)	σ_4	$\Delta\sigma_4$	σ_5	$\Delta\sigma_5$
95.1	0.3	3.4		
105.1	–1.4	5.7		
115.1	6.3	3.6		
125.1	11.9	5.1		
145.1	18.9	5.6		
195.1	27.2	6.4	0.2	1.0
245.1			1.5	0.8
295.1	28.3	5.5	2.2	0.9
395.1	28.5	6.6	2.4	0.8
495.1	29.4	6.7	2.4	0.9
595.1	28.3	7.0	2.4	0.7
695.1			2.3	0.8
795.1	29.1	6.6	3.0	0.8
995.1	26.6	5.5	3.2	0.8
1195.1			3.4	0.7
1495.1	23.1	4.8	3.4	0.8
1995.1	19.9	4.1	3.1	0.7
2495.1	16.4	3.7	2.9	0.6

(13.99 eV; Krisnamurthi *et al* 1991) from these results. For comparison, experimental and theoretical results obtained by different methods are listed in table 3. Good agreement is found between the present result and the other results, which range from 25.45 ± 0.20 eV to 27.8 ± 0.5 eV. Two of them are particularly close to the present one: Pedersen and Hvelplund (1987) obtained (26.6 ± 0.2) eV by electron capture in collisions between slow CO^{2+} ions and a neutral Ne target; Lablanquie *et al* (1989) found the appearance energy to be (26.75 ± 0.50) eV in a photoion–photoion coincidence experiment (PIPICO).

Potential energy curves were calculated by applying various methods: *ab initio* Hartree–Fock (Mazumdar *et al* 1988); configuration–interaction (Wetmore *et al* 1984, Correia *et al* 1985); complete active space self-consistent field and multireference contracted configuration–interaction (Larsson *et al* 1989). As predicted by Hurley (1976), the lowest state of CO^{2+} is commonly agreed to be the $^3\Pi_I$ state. Nevertheless, different calculations disagree for the prediction of the order of higher CO^{2+} states ($^1\Sigma_I^+$, $^1\Pi_I$, $^3\Sigma_I^+$, ...). For instance, Wetmore *et al* (1984) suggested that the $^3\Pi_I$ was followed by the $^1\Pi_I$ and the $^1\Sigma_I^+$ states, whereas some authors reversed this order (Larsson *et al* 1989, Andersen *et al* 1993). Finally, Dawber *et al* (1994) assigned the states in the order defined by Larsson *et al* (1989) (i.e. $^3\Pi_I$, $^1\Sigma_I^+$, $^1\Pi_I$, $^3\Sigma_I^+$) by examining threshold photoelectron coincidence spectroscopy (TEPsCO) data. The observed threshold corresponds to the formation of the three lowest states ($^3\Pi_I$, $^1\Sigma_I^+$ and $^1\Pi_I$) leading to the $C^+(^2P)+O^+(^4S)$ and $C^+(^2P)+O^+(^2D)$ dissociation limits (table 3). The $^3\Sigma_I^-$ state is purely dissociative and also leads to the $C^+(^2P)+O^+(^4S)$ limit.

The presence of a very low signal (around 1.5% of the maximum cross section), observed above 15.1 eV up to the ionization threshold, is difficult to explain. Indeed, this energy range ($\Delta E_e \sim 11.6$ eV) is broader than that observed in the DE or DI processes (Lecointre *et al* 2006). This implies that this low contribution cannot only be explained by the presence of vibrationally excited states in the primary beam nor by any N_2^{2+} contamination ($m/q = 14$), since its appearance potential is 27.9 ± 0.5 eV (Bahati *et al* 2001). Moreover, the N_2^+

Table 3. Energy thresholds for CO^{2+}.

Process	Present thresholds (eV)	Other experimental thresholds (eV)	Experimental method	Molecular state	Theoretical thresholds (eV)	Dissociation limit
$CO^{2+}+2e^-$	26.7 ± 0.5 27.0 ± 0.5[a]	25.45 ± 0.20[b]	Electron loss	$^3\Pi_I$	26.6[e] 27.2[o] 27.2[p]	$C^+(^2P)+O^+(^4S)$
		26.21 ± 0.35[b]	Double electron capture		27.1[e]	
		26.6 ± 0.2[c] 27.0 ± 0.2[d]	Electron capture	$^1\Sigma_I^+$	27.9[o] 27.4[p]	
		26.75 ± 0.50[e] 27.25 ± 0.05[f]	Photon impact		26.5[q]	
		27.31 ± 0.03[g]	Photoionization		27.2[e]	$C^+(^2P)+O^+(^2D)$
		25.90 ± 0.25[h] 26.20 ± 0.25[h] 25.80 ± 0.25[i]	Auger spectroscopy	$^1\Pi_I$	27.75[o] 27.55[p]	
		27.0 ± 2.0[j] 27.5 ± 0.4[k] 27.8 ± 0.5[l]	Electron impact	$^3\Sigma_I^+$	28.5[e] 35.0[o] 29.75[p]	
		27.29 ± 0.01[m] 27.27 ± 0.03[n]	Electron–electron coincidence	$^3\Sigma_I^-$	30.4[e] 30.2[o]	$C^+(^2P)+O^+(^4S)$

[a] Belic *et al* (1997). [b] Mazumdar *et al* (1988). [c] Pedersen and Hvelplund (1987). [d] Herman *et al* (1987). [e] Lablanquie *et al* (1989). [f] Dujardin *et al* (1990). [g] Hochlaf *et al* (1996). [h] Moddeman *et al* (1971). [i] Sieghban *et al* (1969). [j] Tian and Vidal (1999). [k] Newton and Sciamanna (1970). [l] Hille and Märk (1978). [m] Dawber *et al* (1994). [n] Hall *et al* (1992). [o] Wetmore *et al* (1984). [p] Larsson *et al* (1989). [q] Correia *et al* (1985).

dissociative excitation threshold (8.4 ± 0.5 eV) leading to $N^+ + N$ formation is much lower than the present 15.1 eV and it cannot explain this extended energy range.

3.1.2. C^{2+} and O^{2+} production. The absolute cross sections σ_2 and σ_3 are found to have maximum values of $(5.58 \pm 0.55) \times 10^{-18}$ cm^2 and $(1.37 \pm 0.14) \times 10^{-18}$ cm^2, respectively (figure 1). These results are about ten times larger than the result of Belic *et al* (1997). A reanalysis of those previous results indicated that the angular divergence of dissociation products was not properly controlled in that experiment. As a consequence, the transmission factor was systematically overestimated, inducing an important underestimation of the cross section, which explains the above-mentioned discrepancy.

The present C^{2+} and O^{2+} appearance energies are observed to be (43.2 ± 0.5) eV and (53.8 ± 0.5) eV, respectively (table 4). Below the observed thresholds, a small contribution is seen in both cases, which appears approximately above (37.6 ± 0.5) eV for C^{2+} and above (50.1 ± 0.5) eV for O^{2+}. The energy range of these vibrational queues (3.7–6.6 eV) confirms the presence of vibrationally excited states ($v > 10$) in the primary beam as was observed in our previous experiment (Lecointre *et al* 2006) concerning the formation of singly charged ions via DE and DI processes.

For C^{2+}, the present threshold is found to be in good agreement both with our previous result (Belic *et al* 1997) and with those obtained by electron-impact or by photoionization of the CO molecule (Tian and Vidal 1999, Masuoka and Nakamura 1993, Hierl and Franklin 1967). However for O^{2+}, a significant disagreement is observed between the experimental

Table 4. Energy thresholds for C^{2+} and O^{2+}.

Dissociation limit	Present thresholds (eV)	Other experimental thresholds (eV)	Dissociation limit energy (eV)	Estimated KER (eV)[f]
$C^{2+}(^1S)+O(^3P)$	37.6 ± 0.5 43.2 ± 0.5	42.3 ± 1.0[a] 46.0 ± 3.0[b] 42.4 ± 1.0[c] 40.2 ± 0.2[d]	31.8[b] 32.8[e]	10.4 ± 0.5
$C(^3P)+O^{2+}(^3P)$	50.1 ± 0.5 53.8 ± 0.5	48.1 ± 1.0[a] 55.3 ± 3.0[b] 56.0 ± 1.0[c] 47.3 ± 0.3[d]	45.9[b] 46.0[e]	7.8 ± 0.5

[a] Belic *et al* (1997) (electron impact).
[b] Tian and Vidal (1999) (electron impact).
[c] Masuoka and Nakamura (1993) (photoionization).
[d] Hierl and Franklin (1967) (electron impact).
[e] Safvan *et al* (1999) (calculated).
[f] KER values are estimated as the difference between the present thresholds and the corresponding dissociation limit energies (Safvan *et al* 1999).

Table 5. Mean total kinetic energy release ($\overline{\text{KER}}$, eV) for C^{2+} and O^{2+} fragments, at indicated electron energies.

E_e (eV)	40.1[a]	45.1	53.1[a]	55.1	60.1	85.1	145.1	295.1
$C^{2+}+\cdots$	1.2 ± 0.4	4.9 ± 2.1	–	–	9.5 ± 1.0	13.9 ± 0.4	18.4 ± 2.1	20.7 ± 1.2
$O^{2+}+\cdots$	–	–	1.5 ± 0.7	3.0 ± 2.1	3.6 ± 0.2	10.4 ± 0.6	16.2 ± 3.3	24.5 ± 2.1

[a] These data are located in the vibrational queue of the cross section.

thresholds, the present one as well as all the other ones. No definitive argument can be invoked to explain the large dispersion of these results.

Kinetic energy release distributions (KERDs) above the energy threshold are presented for C^{2+} and O^{2+} fragments in figures 2 and 3 respectively, at those selected electron energies where magnetic scans were performed (see section 2.3). The mean total kinetic energy release ($\overline{\text{KER}}$) is also computed (table 5).

Just above the threshold, the KERDs are seen to extend from 0 eV to about 10 eV, both for C^{2+} and O^{2+}, whereas the KERD range extends progressively up to almost 50 eV with increasing incident electron energy. Similarly, the $\overline{\text{KER}}$ values are rising from about 3 to 25 eV. In the vibrational queue (i.e. below the threshold), the KERD is very narrow and the corresponding mean value is only around 1 eV. The KER is roughly estimated, around the threshold, by subtracting the energies related to the $C^{2+}(^1S)+O(^3P)$ and $C(^3P)+O^{2+}(^3P)$ dissociation limits, respectively, from the corresponding appearance potential. The KER values estimated by this approximate method (10.4 and 7.8 eV for C^{2+} and O^{2+}, respectively) are found to correspond to the maximum KER observed at the lowest electron energy available ($E_e = 45.1$ and 55.1 eV, for C^{2+} and O^{2+} in figures 2 and 3, respectively).

Far above the threshold, the present KER values are very large and they continuously increase with incident electron energy. These large KER values indicate that the products result from the dissociation of CO^{3+} molecules (Handke *et al* 1996). These authors also demonstrated that multiply-ionized molecules generally dissociate without proceeding along

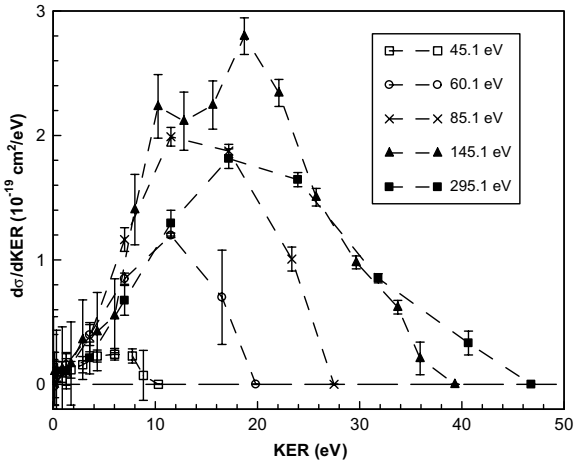

Figure 2. Total kinetic energy release distributions for C^{2+} fragments, for indicated electron energies.

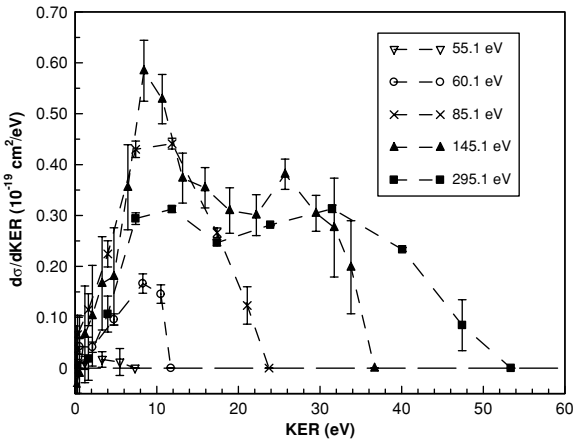

Figure 3. Total kinetic energy release distributions for O^{2+} fragments, for indicated electron energies.

potential curves. This conclusion, which was supported in particular by the experimental results of Tian and Vidal (1999), also explains the unusual KER behaviour observed here as well as the relative importance of σ_2 and σ_3 (see above).

3.2. C^{3+} and O^{3+} production

Absolute cross sections for triply charged fragments formation (σ_4 and σ_5) are found to be very small $(28.3 \pm 7.0) \times 10^{-21}$ cm^2 and $(2.4 \pm 0.7) \times 10^{-21}$ cm^2 around 595 eV (figures 4 and 5 for C^{3+} and O^{3+}, respectively). The attempts to observe triply charged CO^{3+} ions were not successful, the corresponding cross section being estimated to be smaller than 10^{-22} cm^2. As soon as they are formed, these ions dissociate mainly into the $C^{2+} + O^+$ and $C^+ + O^{2+}$ ion pairs (Tian and Vidal 1999). Moreover, these authors estimated the O^{3+} and CO^{3+} signals to be

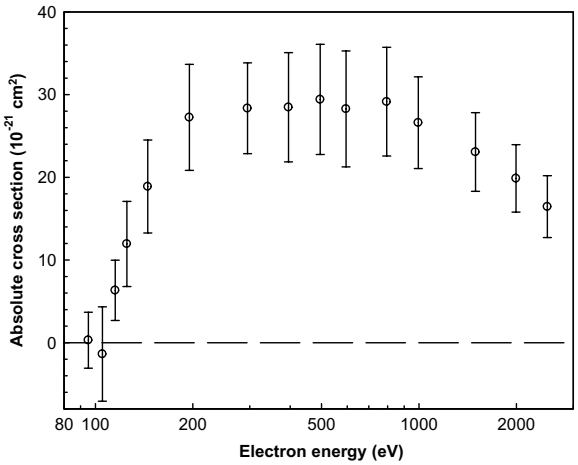

Figure 4. Absolute cross sections for the production of C^{3+} (σ_4, ○) versus electron energy.

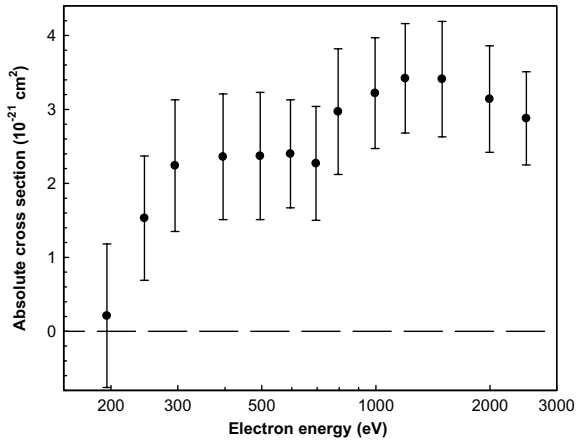

Figure 5. Absolute cross sections for the production of O^{3+} (σ_5, ●) versus electron energy.

negligible. The threshold energies for processes (4) and (5) are estimated to be (107 ± 5) eV and (220 ± 10) eV, respectively (table 6). The observed C^{3+} appearance potential (86 ± 5) eV determined by Tian and Vidal (1999) differs from the present result.

The lowest dissociation limits of C^{3+} + O and C + O^{3+} are 79.6 eV and 100.8 eV (Tian and Vidal 1999), respectively. As mentioned above, the KER are approximated to be about 27 eV and 119 eV, for C^{3+} and O^{3+} respectively, by subtracting the corresponding dissociation limit from the appearance potential. Presently measured KER maxima (63 ± 3 eV and 90 ± 10 eV for C^{3+} and O^{3+}, respectively) are found to be different from the estimated ones. Even so, the corresponding $\overline{\text{KER}}$ (33 ± 5 eV and 39 ± 9 eV for C^{3+} and O^{3+}, respectively) are close to the Coulomb dissociation energies (37.3 eV). This also confirms another conclusion of Handke *et al* (1996) who predicted, in this case, broad KERDs peaked approximately around the Coulombic values.

Table 6. Energy thresholds for C^{3+} and O^{3+}.

Processes	Present thresholds (eV)	Other experimental thresholds (eV)[a]	Dissociation limit energy (eV)[a]	Estimated KER (eV)[b]	Present $\overline{\text{KER}}$ (eV)	Present KER maxima (eV)
$C^{3+} + \cdots$	107 ± 5	86 ± 5	79.6	27 ± 5	33 ± 5	63 ± 3
$O^{3+} + \cdots$	220 ± 10	–	100.8	119 ± 10	39 ± 9	90 ± 10

[a] Tian and Vidal (1999) (electron impact).
[b] KER values are estimated as the difference between the present thresholds and the corresponding dissociation limit energies (Tian and Vidal 1999).

Table 7. Branching ratios for ionization channels.

Fragment	$C^+ + O^+$	CO^{2+}	C^{2+}	O^{2+}	C^{3+}	O^{3+}
Present results	0.86 ± 0.16[a]	0.090 ± 0.004	0.040 ± 0.004	0.010 ± 0.001	$(0.4 \pm 0.1) \times 10^{-3}$	$(3.5 \pm 1.2) \times 10^{-5}$
Tian and Vidal (1999)	0.87 ± 0.17	0.05 ± 0.01	0.05 ± 0.01	0.020 ± 0.003	$(1.2 \pm 0.3) \times 10^{-3}$	Negligible
Masuoka and Nakamura (1993)	0.84 ± 0.08	0.039 ± 0.004	0.11 ± 0.01	0.015 ± 0.001	–	–
Hitchcock *et al* (1998)	0.83 ± 0.21	0.03 ± 0.01	0.09 ± 0.02	0.06 ± 0.02	Negligible	Negligible

[a] Lecointre *et al* (2006).

The binding energies of C(1s) and O(1s) electrons in CO^+ should be close to those in CO (296.2 and 542.3 eV; Thomas 1970). Ejection of one of these electrons results in an Auger process, which should explain the extended maximum of the cross section observed around 300 eV for C^{3+} (figure 4). For O^{3+}, the strong structure which appears above 700 eV (figure 5) is probably also due to the Auger process, though the O(1s) binding energy is slightly smaller than the observed threshold.

3.3. Branching ratios

The branching ratio (R_n) in favour of a particular process n is evaluated as follows:

$$R_n = \frac{\sigma_n}{\sigma_\mathrm{I}} \tag{15}$$

where σ_I is the total ionization cross section calculated by summing all the contributing absolute ionization cross sections around the cross section maximum. Present results and other experimental works are summarized in table 7. Tian and Vidal (1999) studied all the possible dissociation channels for double ionization of CO and the corresponding branching ratios are determined close to the maximum cross section ($E_\mathrm{e} = 150$ eV). Hitchcock *et al* (1998) and Masuoka and Nakamura (1993) analysed the relative importance of CO ionization reactions following high-energy photo-absorption. Table 7 lists only the branching ratios estimated at the highest photon energy available (534 eV and 100 eV, respectively). For single ionization (CO^{2+}), the present result ($R_\mathrm{SI} = 0.09$) is about twice that of the three others (0.03–0.05), due to the shorter time of flight of these ions in the present experiment. The data agree all together on confirming the predominance of the $C^+ + O^+$ process ($R_\mathrm{DI} \sim 0.85$). For charge states 2 and 3, the carbon formation is favoured with respect to that of oxygen, as expected, because of the lower dissociation limit for carbon products. The branching ratios for the formation of triply charged ions are extremely small and most of them are estimated to

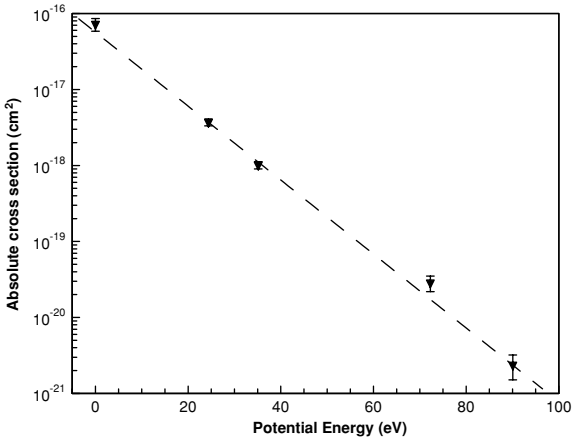

Figure 6. Present absolute cross sections (▼) for individual ion pair formation ($C^+ + O^+$, $C^{2+} + O^+$, $C^+ + O^{2+}$, $C^{3+} + O^+$ and $C^+ + O^{3+}$) as a function of the corresponding potential energy at the dissociation limit for $E_e = 395$ eV. The dashed line is the result of the fit (equation (16)).

be negligible by other authors, except for the C^{3+} formation for which present result is about one third of the one of Tian and Vidal (1999).

Handke *et al* (1996) concluded that the ionization channels with a lower dissociation limit have a higher preference, an observation that is confirmed by the present experiment as well as by others. This suggests that the cross sections strongly depend on the potential energy (E_p) of each dissociated ion pair. This dependence is clearly established in figure 6 where the cross sections, measured at 395 eV, are plotted as a function of the potential energy. The $C^+ + O^+$ limit is defined as the zero potential energy. In a semi-log scale, the cross section exhibits a remarkably linear behaviour, which is accurately reproduced by the following fitting function:

$$\sigma = \sigma_0 \, e^{-(E_p/E_{p_0})} \tag{16}$$

where the two fitting parameters are estimated to be $\sigma_0 = 5.7 \times 10^{-17}$ cm^2 and $E_{p_0} = 8.9$ eV. It will be interesting to develop a similar analysis for other molecules in order to check for the general character of expression (16) and for the physical meaning of the fitting constant E_{p_0}.

3.4. Calculated ionization cross sections

A recently described variant of the Deutsch–Märk (DM) formalism (Deutsch *et al* 2006) is used to calculate the total CO^+ ionization cross section. This modified DM formula is applicable to molecular ions and describes the 'ionic' component of the molecular ion by 'ionic' weighting factors in the cases where the positive charge (i.e. the 'missing' electron in the ion) can be localized. This approach was first used in the case of $C_2H_2^+$ (Deutsch *et al* 2006), where the missing electron is essentially 100% localized at the site of a C atom, and yielded a calculated cross section that was in excellent agreement with recent experimental data (Belic *et al* 2003, Cherkani-Hassani *et al* 2004).

Following the procedure discussed in detail in the paper of Deutsch *et al* (2006), Mulliken population analyses for CO and CO^+ revealed that the ionization of CO proceeds predominantly by removing an electron from a C(2s) orbital. The 'missing' electron in CO^+ can be attributed to almost 90% to the C(2s, 2p) orbitals and only to about 10% to the O(2s,2p) orbitals. Thus,

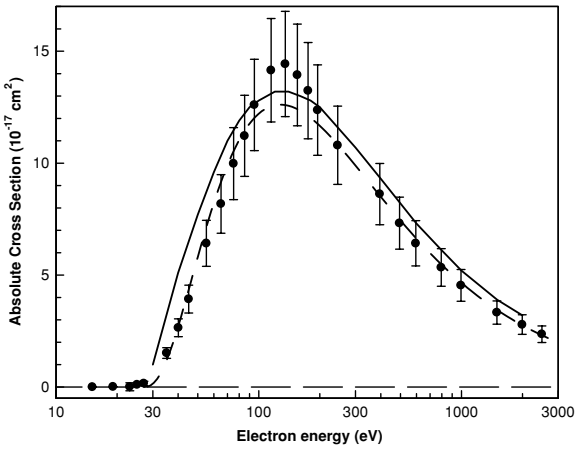

Figure 7. Calculated absolute cross section (σ_I) for the total ionization of CO^+ as a function of electron energy using the present DM formalism (——) in comparison with present experimental data (•) and a calculated BEB cross section (— —) (Kim *et al* 2000).

the ionic character of CO^+ can be largely, but not exclusively identified with a C^+ ion. In the present calculation, the ionic weighting factors are now used for both C^+ and O^+ apportioned according to the CO^+ population analysis. The weighting factors for the C^+ ion were taken from Deutsch *et al* (2006) and the weighting factors for O^+ were determined by fitting a DM cross section to the experimentally determined cross section for the process $e^- + O^+ \rightarrow O^{2+} + 2e^-$ (Tawara and Kuto 1999).

Figure 7 shows a comparison of the present calculation of the total CO^+ ionization cross section in comparison with the experimentally determined cross section σ_I and a calculated BEB cross section of Kim *et al* (2000). It is apparent from figure 7 that the present calculation and the BEB cross section reproduce the measured cross section shape quite well up to 100 eV. The present calculation is consistent with the measured cross section maximum, but it slightly exceeds the measured data for energies below 80 eV and above 200 eV. In contrast, the BEB calculation has a maximum value that lies about 15% below the maximum of the measured cross section, but agrees with the measured cross section shape above 300 eV.

While the agreement between present calculation and the measured cross section in the case of CO^+ is perhaps not quite as good as in the earlier case of the $C_2H_2^+$ ion, the present calculation for CO^+ nevertheless shows the same trends, good agreement with the measured data at low impact energies, satisfactory agreement in the range of the cross section maximum, and an overestimation at higher impact energies. Perhaps more importantly, the present calculations demonstrate that the localization of the 'missing' electron in conjunction with the proper use of ionic weighting factors significantly improves the level of agreement between experiment and calculation.

One can note here that the BEB calculation as described by Kim *et al* (2000) has been modified by the author from its original form, which is applicable to neutral targets, to a form that was found more suitable for ionic targets. This was done by introducing rather arbitrarily a factor of '1/2' in the denominator of one of the quantities in the BEB cross section formula (for details, see equation (2) in the paper by Kim *et al* (2000) and its discussion). As stated by the author, this universal factor '1/2' (which was not justified in terms of any underlying physics argument) resulted in a better agreement of the thus modified BEB cross section with experimental data, particularly in the low-energy region.

4. Summary

Absolute cross sections for electron impact ionization of CO^+, leading to the formation of doubly and triply charged products (CO^{2+}, C^{2+} and O^{2+}, C^{3+} and O^{3+}) are reported in the energy range from their respective thresholds to 2.5 keV. The analysis of ionic fragment velocity distributions allows the determination of the kinetic energy release for dissociation products, at selected electron energies. Present energetic results (thresholds and KERs) are compared with published experimental or theoretical data and, overall, good agreement is found. At a given incident electron energy, the cross sections are seen to decrease exponentially with respect to the potential energy of each dissociated ion pair. The present experimental work supports most of the conclusions of the theory formulated by Handke *et al* (1996), especially concerning the role of the dissociation potential energy. The cross sections estimated by application of the Deutsch–Märk (DM) model for ionization are found to agree with the experimental results.

Acknowledgments

The authors acknowledge the financial support of the Association Euratom-Belgian State and the technical support of C Alaime and D Dedouaire. They are indebted to the Forschungszentrum Jülich for the lending of the ECR ion source. The content of the publication is the sole responsibility of its publishers and it does not necessarily represent the views of the EU Commission or its services. It was partially supported by the FWF, Wien, Austria and the EU Commission, Brussels. J Limtrakul acknowledges the support from the TRF Senior Research Fund, the Ministry of University Affairs under the Science and Technology Higher Education Development Project and the Kasetsart University Research and Development Institute. K Becker acknowledges partial financial support from the US National Aeronautics and Space Administration (NASA) under grant NNG04GR07G.

References

Andersen L H, Posthumus J, Vahtras O, Agren H, Elander N, Nunez A, Scrinzi A, Natiello M and Larsson M 1993 *Phys. Rev. Lett.* **71** 1812

Bahati E M, Jureta J J, Belic D S, Cherkani-Hassani H, Abdellahi M and Defrance P 2001 *J. Phys. B: At. Mol. Opt. Phys.* **34** 2693

Belic D S, Cherkani-Hassani H and Defrance P 2003 *23th ICPEAC, Book of Abstracts, FR079 (Stockholm, Sweden)*

Belic D S, Yu D J, Siari A and Defrance P 1997 *J. Phys. B: At. Mol. Opt. Phys.* **30** 5535

Brehm B and de Frênes G 1978 *Int. J. Mass Spectrom. Ion Phys.* **26** 251

Cherkani-Hassani H 2004 *PhD Thesis* Université Catholique de Louvain

Correia N, Flores-Riveros A, Agren H, Helenelund K, Asplund L and Gelius U 1985 *J. Chem. Phys.* **83** 2035

Curtis J M and Boyd R K 1984 *J. Chem. Phys.* **80** 1150

Cuthbert J, Farren J F, Prahallada Rao B S and Preece E R 1966 *Proc. Phys. Soc.* A **88** 91

Dawber G, McConkey A G, Avaldi L, MacDonald M A, King G C and Hall R I 1994 *J. Phys. B: At. Mol. Opt. Phys.* **27** 2191

Defrance P, Brouillard F, Claeys W and Van Wassenhove G 1981 *J. Phys. B: At. Mol. Phys.* **14** 103

Deutsch H, Becker K, Defrance P, Probst M, Limtrakul J and Märk T D 2006 *Eur. Phys. J.* D **38** 489

Dorman F H and Morrison J D 1961 *J. Chem. Phys.* **35** 575

Dujardin G, Hellner L, Hamdan M, Brenton A G, Olsson B J and Besnard-Ramage M J 1990 *J. Phys. B: At. Mol. Opt. Phys.* **23** 1165

Hall R I, McConkey A G, Avaldi L, MacDonald M A and King G C 1992 *J. Phys. B: At. Mol. Opt. Phys.* **25** 411

Handke G, Tarantelli F and Cederbaum L S 1996 *Phys. Rev. Lett.* **76** 896

Herman Z, Jonathan P, Brenton A G and Beynon J H 1987 *Chem. Phys. Lett.* **141** 433

Hierl P M and Franklin J L 1967 *J. Chem. Phys.* **47** 3154

Hille E and Märk T D 1978 *J. Chem. Phys.* **69** 4600

Hirsch R G, Van Brunt R J and Writehead W D 1975 *Int. J. Mass Spectrom. Ion Phys.* **17** 335

Hitchcock A P, Lablanquie P, Morin P, Lizon E, Lugrin A, Simon M, Thiry P and Nenner I 1998 *Phys. Rev.* A **37** 2448
Hochlaf M, Hall R I, Penent F, Kjeldsen H, Lablanquie P, Lavollée M and Eland J H D 1996 *Chem. Phys.* **207** 159
Hurley A C 1976 *J. Chem. Phys.* **42** 335
Kim Y K, Irikura K K and Ali M A 2000 *J. Res. Natl Stand. Technol.* **105** 285
Krisnamurthi V, Nagasha K, Marate V R and Mathur D 1991 *Phys. Rev.* A **44** 5460
Lablanquie P *et al* 1989 *Phys. Rev.* A **40** 5673
Larsson M, Olsson B J and Sigray P 1989 *Chem. Phys.* **139** 457
Lecointre J, Belic D S, Cherkani-Hassani H, Jureta J J and Defrance P 2006 *J. Phys. B: At. Mol. Opt. Phys.* **39** 3275
Liu W and Victor A G 1994 *Astrophys. J.* **435** 909
Lotz W 1968 *Z. Phys.* **216** 241
Masuoka T and Nakamura E 1993 *Phys. Rev.* A **48** 4379
Mazumdar S, Rajgara F A, Marathe V R, Badrinathan C and Mathur D 1988 *J. Phys. B: At. Mol. Opt. Phys.* **21** 2815
Moddeman W E, Carlson T A, Krause M O, Pullen B P, Bull W E and Schweitzer G K 1971 *J. Chem. Phys.* **55** 2317
Newton A S and Sciamanna A F 1970 *J. Chem. Phys.* **53** 132
Pedersen J O K and Hvelplund P 1987 *J. Phys. B: At. Mol. Phys.* **20** L317
Safvan C P, Jensen M J, Pedersen H B and Andersen L H 1999 *Phys. Rev.* A **60** R3361
Sieghban K *et al* 1969 *ESCA Applied to free Molecules* (Amsterdam: North-Holland) p 76
Tawara H and Kuto M 1999 *Research Report, NIFS—Data Series Report 51*
Tian C and Vidal C R 1999 *Phys. Rev.* A **59** 1955
Thomas T D 1970 *J. Chem. Phys.* **53** 1744
Wetmore R W, Le Roy R J and Boyd R K 1984 *J. Phys. Chem.* **88** 6318